Coseismic and postseismic deformation due to the 2007 *M*5.5 Ghazaband fault earthquake, Balochistan, Pakistan

H. Fattahi[1], F. Amelung[1], E. Chaussard[2], and S. Wdowinski[1]

[1]Rosenstiel School of Marine and Atmospheric Science, University of Miami, Miami, Florida, USA, [2]Department of Earth and Planetary Science, University of California, Berkeley, California, USA

Abstract Time series analysis of interferometric synthetic aperture radar data reveals coseismic and postseismic surface displacements associated with the 2007 *M*5.5 earthquake along the southern Ghazaband fault, a major but little studied fault in Pakistan. Modeling indicates that the coseismic surface deformation was caused by ~9 cm of strike-slip displacement along a shallow subvertical fault. The earthquake was followed by at least 1 year of afterslip, releasing ~70% of the moment of the main event, equivalent to a *M*5.4 earthquake. This high aseismic relative to the seismic moment release is consistent with previous observations for moderate earthquakes (*M* < 6) and suggests that smaller earthquakes are associated with a higher aseismic relative to seismic moment release than larger earthquakes.

1. Introduction

Since 1892 four *M* > 7 earthquakes ruptured the western India plate boundary [*Ambraseys and Bilham*, 2003], the latest one being the 2013 *M*7.7 earthquake [*Avouac et al.*, 2014; *Barnhart et al.*, 2014; *Jolivet et al.*, 2014b]. The Ghazaband fault, one of the main structures of the western India plate boundary zone, is a possible source of the *M*7.7 1935 earthquake which devastated the city of Quetta causing up to 35,000 fatalities [*Lawrence et al.*, 1981; *Ambraseys and Bilham*, 2003; *Szeliga et al.*, 2012].

Geodetic observations of strain accumulation and release can help to better understand the nature of the Ghazaband fault and the earthquake hazard of Balochistan. Here we report interferometric synthetic aperture radar (InSAR) observations of the coseismic and postseismic deformation associated with the *M*5.5 earthquake of 19 October 2007. We estimate the ratio of aseismic moment release by afterslip relative to the coseismic moment release and compare the ratio with other earthquakes with reported observations of afterslip.

2. Tectonic Setting

The Chaman fault system, forming the transform to transpressive boundary between the India and Eurasia tectonic plates, consists of a group of sinistral strike-slip faults including the Ornach Nal, Ghazaband, and Chaman faults (Figure 1a). To the south, the Chaman fault connects with the faults of the Makran ranges (Siahan, Panjgur, and Hoshab faults), which accommodate both the shortening due to the convergence of Arabia and Eurasia and the shear between India and Eurasia. The Ghazaband fault runs for about 300 km roughly parallel to the Chaman fault.

Szeliga et al. [2012] report velocities from a sparse campaign GPS network at latitudes 30–32°N. Their stations KACH and CHMC suggest ~12 mm/yr relative velocity across the combined Chaman and Ghazaband fault systems. However, plate motion models suggest 26 mm/yr fault-parallel and 5–8 mm/yr fault-normal motion between the Indian and the Eurasian plates [*Szeliga et al.*, 2012].

Four moderate earthquakes (5 < *M* < 6) with predominantly strike-slip focal mechanisms occurred in 1975, 1978, 1990, and 2007 in the southern Ghazaband fault area near latitude 28.5°N (Figure 1a). In 1993 a *M*5.5 earthquake ruptured the northern Ghazaband fault near the city of Pishin [*Szeliga*, 2010]. These earthquakes are evidence that the fault accommodates a portion of the deformation.

The Global centroid moment tensor (CMT) and U.S. Geological Survey solutions place the 19 October 2007 event 15 km northeast of the observed ground deformation likely due to location error given the poor
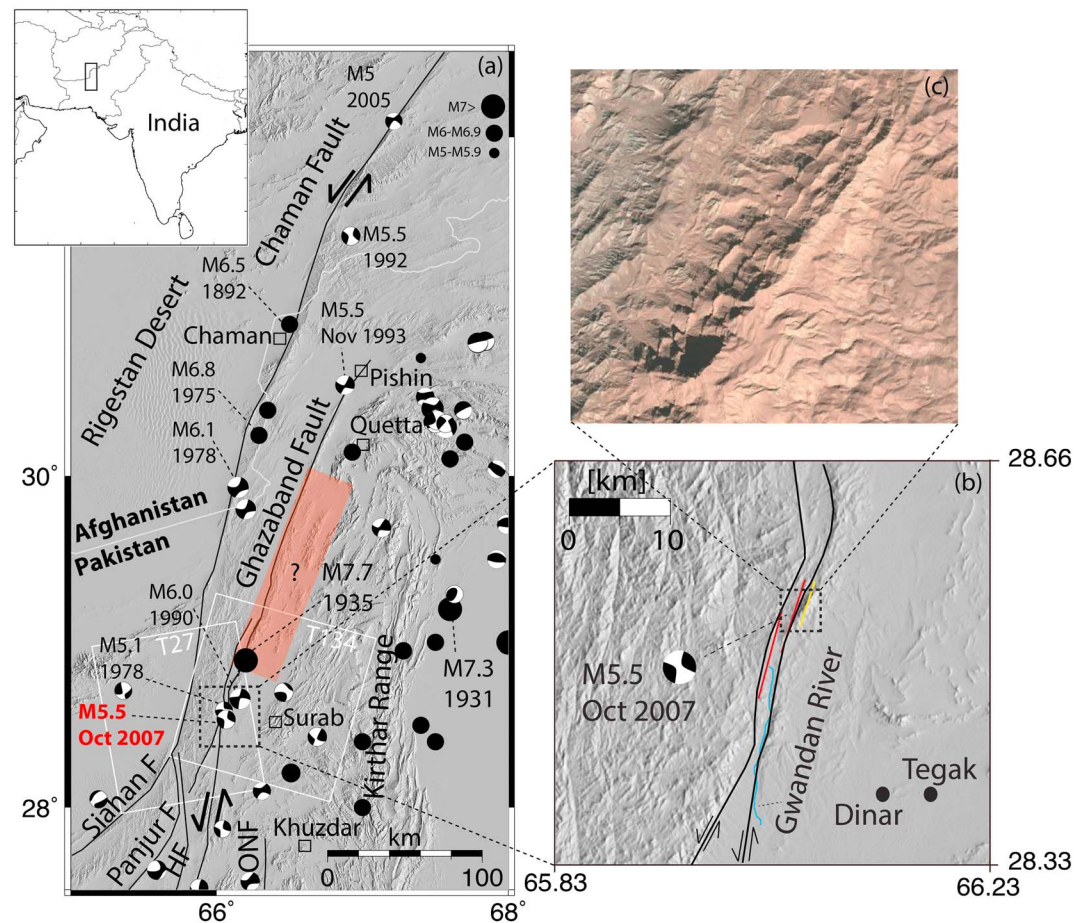
Figure 1. (a) Location map of the Ghazaband fault. Solid white rectangles: footprint of ascending and descending frames. Black circles show the 1982–1976, $M > 5$ earthquakes from *Ambraseys and Bilham* [2003]. Focal mechanisms are from the Global CMT catalog. Locations of ~ M7.7 1935 Quetta earthquake and M6.1 1978 Nushki earthquake on Chaman fault are from *Engdahl and Villaseñor* [2002] and location of M5 2005 earthquake on Chaman fault north of Chaman city is adjusted from *Furuya and Satyabala* [2008]. Faults at latitude <29°N are from *Lawrence et al.* [1981] and for >29°N derived from Google Earth imagery. Orange shaded rectangle: possible location of 1935 rupture. HF and ONF stand for Hoshab Fault and Ornach Nal Fault, respectively. (b) Zoom into epicentral area of the M5.5 October 2007 earthquake. Red lines are strike-slip dislocations, yellow line is reverse-slip dislocation, and blue line is the Gwandan River. (c) Optical imagery from Google Earth of the mountain range overlying the reverse-slip dislocation (see text).

resolution of global seismic networks [*Weston et al.*, 2011]. The earthquake was followed by a M3.9 aftershock 1 day later. The topography of the epicentral region and Google Earth imagery suggests for this latitude a system of two subparallel faults (Figure 1b).

3. Data Analysis and Results

We use 2004–2010 ascending (beam IS6) and descending (beam IS2) Envisat advanced synthetic aperture radar (ASAR) data from tracks 27 and 134 to investigate the coseismic and postseismic ground deformation due to the 2007 earthquake using InSAR time series analysis. We use the Jet Propulsion Laboratory/Caltech ROI_PAC software [*Rosen et al.*, 2004] for processing interferograms with perpendicular baselines less than 200 m. We invert the network of interferograms (supporting information Figure S1) for the phase history [*Berardino et al.*, 2002] and then correct for the local oscillator drift of the ASAR instrument [*Marinkovic and Larsen*, 2013; *Fattahi and Amelung*, 2014], for topographic residuals [*Fattahi and Amelung*, 2013] and for the stratified tropospheric delay [*Jolivet et al.*, 2014a] using the ERA-Interim global atmospheric reanalysis model [*Dee et al.*, 2011]. From the corrected
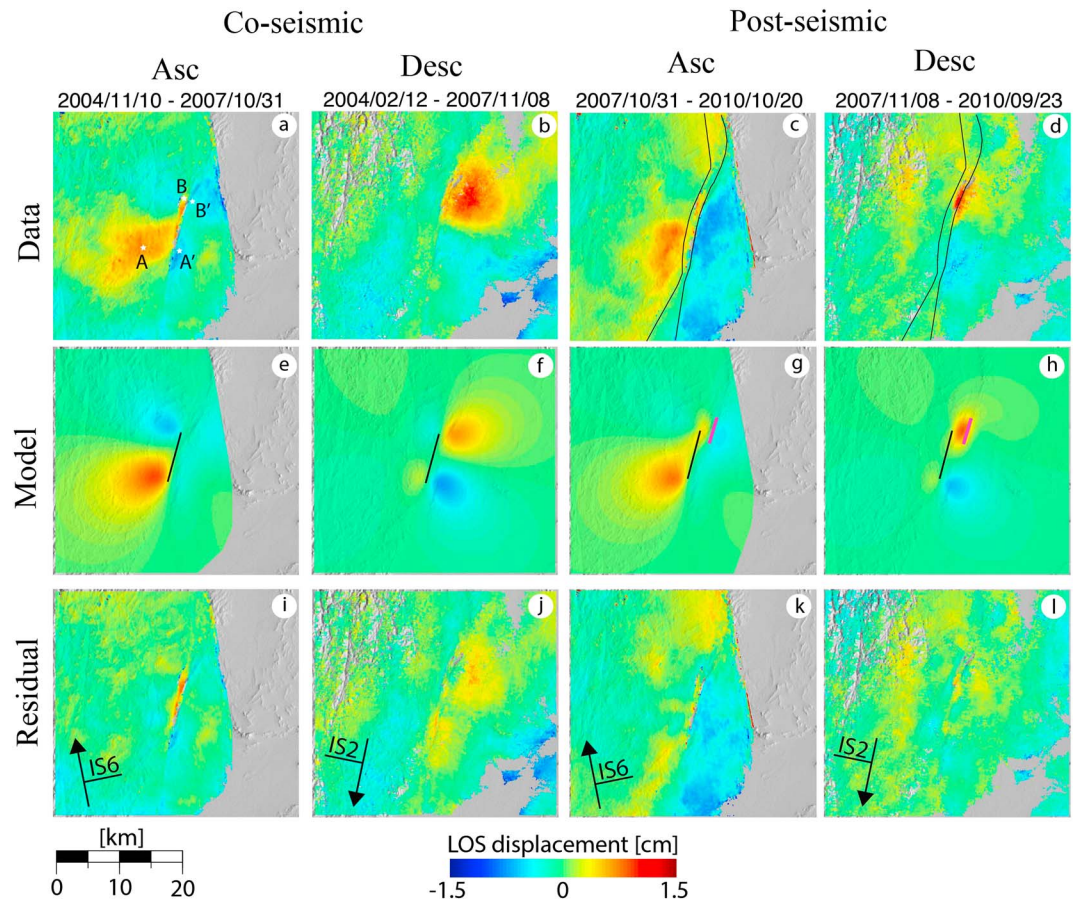
Figure 2. (a, b) Coseismic and (c, d) postseismic LOS displacement maps obtained from the time series for the Ghazaband fault earthquake from ascending and descending Envisat satellite tracks (IS6 and IS2 beams, respectively). (e–h) Predicted LOS displacements from the best fitting models. Black and pink lines are modeled strike-slip and dip-slip dislocations, respectively. (i–l) Differences between the best fitting models and the observations (residuals). Arrows show satellite flight directions, and black bars show the look directions. The location is given by Figure 1b.

InSAR time series we reconstruct the coseismic and postseismic displacements without any assumption about the spatial or temporal deformation model.

Coseismic ground displacement maps in radar line-of-sight (LOS) direction between 2004 and 12 and 20 days after the earthquake obtained from the ascending and descending displacement histories show the ground deformation during and in the first days after the earthquake (Figures 2a and 2b). We present displacements since 2004 because these early acquisitions are characterized by smaller lateral tropospheric delay variations. The ascending LOS displacement map shows the typical quadruple displacement pattern of strike-slip earthquakes. The displacement toward the satellite in the southwestern lobe (positive LOS, red colors, Figure 2a) and away from the satellite in the northeastern lobe (negative LOS, blue colors) is consistent with left-lateral displacement along a NNE trending fault, similar for the descending data, but the displacement lobes have opposite signs.

Postseismic displacement maps for the subsequent 3 year period show similar deformation patterns, suggesting afterslip with sign and magnitude comparable to the coseismic slip. This is further supported by the similarity of the east-west and vertical displacement patterns inferred from combination of the ascending and descending data (Figure S2). However, the postseismic vertical displacement field shows a notable difference in the elongated uplift in the northeast (Figure S2d), which is referred to in the following as the northeastern uplift. This uplift is likely due to afterslip rather than poroelastic deformation, which would result in ground subsidence [*Peltzer et al.*, 1998; *Fielding et al.*, 2009].

Table 1. Best Fitting Model Parameters for the Coseismic and Postseismic Displacements[a]

Fault Number	Longitude	Latitude	Length (km)	Width (km)	Depth (km)	Strike	Dip	Strike Slip (cm)	Dip Slip (cm)	M	Total M
				Coseismic							
1	66.03	28.50	7.7 ± 0.8	8.0 ± 2	1.7 ± 0.4	15°	−90°	9.0 ± 2	0	5.48 ± 0.03	5.48 ± 0.03
				Postseismic							
1	66.03	28.50	8.8 ± 0.5	6.0 ± 1.2	1.3 ± 0.3	15°	−90°	7.0 ± 1	0	5.35 ± 0.02	5.4 ± 0.02
2	66.06	28.53	4	4	2	17.9°	−83° ± 2.6°	0	3.0 ± 1	4.8 ± 0.01	

[a]The uncertainties were derived from the posterior density distribution of the fault parameters obtained from the Gibbs sampling algorithm (see supporting information Figures S3 and S4 for the plots of the posterior density distribution). To calculate the moment magnitude, we assume rigidity equal to 3E10 Pa.

4. Modeling

We use uniform dislocations in a homogeneous elastic half-space to infer the fault slip responsible for the surface displacements. Our data set consists of 2500 pixels of the LOS displacements sampled from a uniform grid for each viewing geometry. We use a Gibbs sampling inversion technique to determine the parameters and uncertainties of the dislocations [_Brooks and Frazer_, 2005].

For the coseismic observations, we consider a single vertical strike-slip dislocation. We fix the location and strike of the fault and invert for the best fitting fault length, width, depth, and displacement of the dislocation. The coseismic observations are best explained by ~9 cm of strike-slip displacement along a ~7.7 km long fault at depth (top of the fault) of ~1.7 km (Table 1).

For the postseismic observations the model consists of a strike-slip dislocation with the location of the coseismic model (fault 1) and a dip-slip dislocation (fault 2). We invert for the displacement, depth, length, and width of fault 1 and for the dip and dip-slip displacement of fault 2. The residual atmospheric noise in the InSAR data and the small displacement signal does not allow to constrain the length, width, and depth of the second dislocation. The moment release from fault 2 is only 7% of the total postseismic moment release (Table 1). The postseismic observations are best explained by ~7 cm left-lateral displacement for fault 1 and by ~3 cm reverse slip along fault 2 at depths of ~1.3 and ~2 km, respectively (Table 1 and Figures 2g and 2h). The marginal posterior density distributions (PDDs) for the estimated fault parameters (supporting information Figures S3 and S4) show that the fault source parameters have roughly Gaussian distributions.

For the coseismic data, the ascending residual map shows a narrow strip of LOS displacement very close to the fault (Figure 2i), which occurs probably because local fault slip variations are not represented by the uniform dislocation. The descending data, which are not sensitive to along-strike fault displacements (the radar looks nearly perpendicular to the fault), do not have such residuals. The residuals in the NE lobe of the descending data (Figure 2j) may be due to early afterslip as it spans eight more days than the ascending data. The residuals in Figure 2k (the blue color at the bottom) are most likely due to the residual tropospheric delay in the data.

5. Discussion

The InSAR data provide insights into a tectonically complex section of the Ghazaband fault system. Coseismic ground deformation was caused by shallow slip along a subvertical, left-lateral, strike-slip fault and postseismic deformation by slip along the same fault as well as by dip slip on a neighboring thrust fault. The geodetic moment magnitude of ~ _M_5.5 is consistent with the seismic moment magnitude of _M_5.5 from the Global CMT catalog.

5.1. Shallow Slip

The earthquake was associated with coseismic and postseismic fault slip at shallow depth (~1 to 2 km depth of the model dislocation upper edges). Shallow slip was also observed in the 1993 _M_5.5 earthquake along the northern strand of the Ghazaband fault (focal depth of 2.25 km [_Szeliga_, 2010]) and in the 2005 _M_5.0 Chaman fault earthquake (maximum slip depth of 2 km [_Furuya and Satyabala_, 2008]). The 2013 _M_7.7 Balochistan earthquake also largely ruptured near the surface [_Avouac et al._, 2014], as did several historic earthquakes
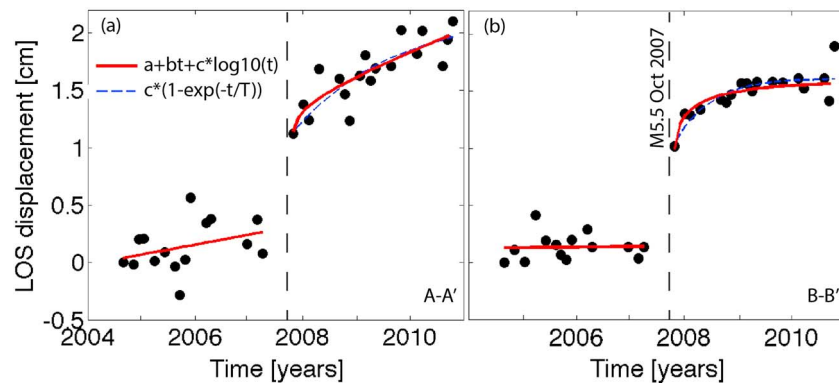
Figure 3. Relative ascending LOS displacement histories across the fault for (a) the southwestern deformation lobe between points A and A' and (b) the northeastern uplifting area between points B and B' (see Figure 2a for locations), together with the linear fits for the preseismic and the logarithmic and exponential fits to the postseismic data.

along the Chaman fault [*Szeliga et al.*, 2012]. This could suggest that shallow fault slip is widespread in this plate boundary zone, in contrast to other tectonic settings where some earthquakes may be associated with slip deficits at shallow depth [*Fialko et al.*, 2005; *Dolan and Haravitch*, 2014]. Shallow slip deficit can be partly explained by shallow creep distributed across the fault during the interseismic period [*Kaneko and Fialko*, 2011] or by distributed yielding [*Lindsey et al.*, 2014]. *Xu et al.* [2015] suggest that the shallow slip deficit is apparent and an artifact due to interferometric decorrelation near earthquake ruptures. This interpretation is consistent with the presence of shallow slip and high interferometric coherence near the Ghazaband fault trace.

5.2. Afterslip

The InSAR data and modeling show that the earthquake was followed by 7 cm of slip along the strike-slip fault and by 3 cm of slip along the shallow thrust fault (Table 1). The LOS displacement histories for the southwestern deformation lobe and for the northeastern uplift area, relative to points on the opposite sides of the fault, show the displacements before, during, and after the earthquake (Figures 3a and 3b). The AA' displacement history is noisier than the BB' displacement history because the distance between the points is larger, and therefore, the difference is more affected by the residual atmospheric delay. The slight slope of less than 0.5 mm/yr of the AA' displacement history is most likely due to the noise of the InSAR data and not due to the interseismic shallow fault creep, as confirmed by the absence of a trend in the less noisy BB' displacement. The afterslip lasted over 2 years in the southeastern area (Figure 3a) and at least 1 year in the northeastern area (Figure 3b). The postseismic displacement histories are well fitted by logarithmic or exponential functions. This 2007 Ghazaband fault earthquake has a ratio of $70 \pm 10\%$ between postseismic and coseismic moment release, which is a lower bound estimate given that the first 12 days and 20 days of afterslip are included in the coseismic displacement from ascending and descending data, respectively.

Space-geodetic observations of afterslip over the past two decades provide an opportunity to better understand the nature of afterslip. Afterslip generally surrounds the high-slip patches of the coseismic rupture [*Marone et al.*, 1991; *Perfettini and Avouac*, 2007] and has been observed following strike-slip [*Freed*, 2007; *Furuya and Satyabala*, 2008; *Hearn et al.*, 2009], thrust [*Podgorski et al.*, 2007], and normal crustal earthquakes [*Hamiel et al.*, 2012], following subduction earthquakes [*Miyazaki et al.*, 2004; *Hsu et al.*, 2006; *Sun et al.*, 2014] and following a detachment fault earthquake [*Owen and Bürgmann*, 2006].

Figure 4 shows the ratio of the aseismic moment release by afterslip relative to the coseismic moment release for 22 earthquakes in different tectonic settings (references are in Table S1). The ~70% ratio for the *M*5.5 on the Ghazaband fault falls below the ratios of 500%, 280%, and 300% for the *M*5 2005 Chaman fault, the *M*6 2004 Parkfield, California, and the *M*4.7 2008 Mogul, Nevada, earthquakes, respectively [*Freed*, 2007; *Furuya and Satyabala*, 2008; *Bell et al.*, 2012], and above the ratios of 15%, 2%, and 29–32% for the *M*7.3 1992 Landers, *M*7.1 1999 Hector Mine, and *M*7.5 1999 Izmit, Turkey, earthquakes, respectively [*Shen et al.*, 1994; *Jacobs et al.*, 2002; *Wang et al.*, 2009]. The distribution shows that moderate earthquakes (*M* < 6) are
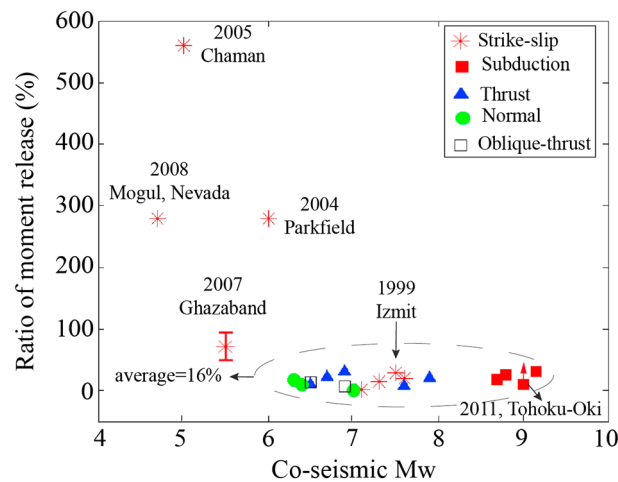
Figure 4. Ratio of aseismic moment release by afterslip relative to the coseismic moment release for earthquakes with reported afterslip (see supporting information Table S1). The red bar for the Ghazaband earthquake shows the 2σ uncertainty. The red arrow for the 2011 Tohoku-Oki earthquake indicates that afterslip still continues and the ratio will increase with future observations.

followed by proportionally more aseismic moment release than large earthquakes ($M > 6$). This difference could reflect that large earthquakes produce a more complete stress drop than smaller ones, and thus, proportionally less elastic strain energy remains stored in the crust. We note that these ratios have to be interpreted with caution because many studies lack continuous geodetic observations immediately after the earthquake and because afterslip may continue for many years at a decaying rate such as for the Izmit earthquake [*Çakir et al.*, 2012].

5.3. Depths of Coseismic Slip and Afterslip

The PDDs of the depths of the upper edge of the dislocations estimated using the Gibbs sampling approach show that the postseismic dislocation is slightly shallower

than the coseismic dislocation (means of 1.3 and 1.7 km, respectively, Figure 5). This, together with the smaller width of the postseismic dislocation (6 km for the postseismic versus 8 km for the coseismic dislocation, Table 1), suggests that the afterslip was generally shallower than the coseismic slip, consistent with the narrower spatial pattern of the postseismic (Figure S2b) compared to the coseismic surface displacements (Figure S2a). The shallower depth of afterslip is consistent with inferred velocity-strengthening behavior along the shallow parts of faults related to a lower degree of sediment consolidation [*Scholz*, 1998; *Wei et al.*, 2013]. However, the small difference between the depths of the coseismic and postseismic dislocations (Figure 5) suggests possible overlap between the coseismic and postseismic patches. The overlap of the coseismic and postseismic regions can represent conditionally stable frictional behavior of the shallower parts of the fault with coseismic slip nucleated on velocity-weakening asperities at depth and propagated to the conditionally stable regions, which can also slip aseismically [*Scholz*, 1998; *Noda and Lapusta*, 2013]. However, the small surface displacement signal does

not allow to infer the spatial variation of slip at depth, and thus, we cannot rule out an alternative scenario of lateral variations in frictional behavior with seismic movements of velocity-weakening patches and aseismic movements of velocity-strengthening patches [e.g., *Hsu et al.*, 2006].

5.4. Postseismic Push-Up

The reverse-slip dislocation explaining the postseismic uplift is located under a ~7 km long unnamed mountainous ridge subparallel to the Ghazaband system (Figure 1b). The ridge is the highest topographic expression in the area (with elevation of ~300 m above the surroundings). The spatial match with the detected uplift suggests that the ridge may have been created by repeated push-ups similar to the 2007 event. Inspection of optical remote sensing imagery (Google Earth imagery) shows that the ridge is the only location in the region where inclined sedimentary strata are exposed at the surface (Figure 1c). This

Figure 5. Marginal posterior density distribution for the depth of coseismic (red) and postseismic (blue) dislocations.

suggests erosional unroofing of recent uplift and that the ridge is the geomorphic expression of the contractional deformation associated with a restraining stepover of the Ghazaband fault system and/or transpressional tectonics.

6. Conclusions

Modeling the InSAR observations for the M5.5 October 2007 earthquake on the southern end of the Ghazaband fault suggests that the coseismic slip was produced by ~9 cm of left-lateral displacement on a shallow subvertical fault. The earthquake was followed by ~7 cm slip above and along the main rupture and by a few centimeters of triggered slip along a nearby thrust fault. The InSAR time series shows that afterslip lasted for at least 1 year and released ~70% of the moment of the main event. This ratio between aseismic and seismic moment release is consistent with previous observations of high aseismic moment release for moderate earthquakes ($M < 6$) and higher than the ratio for larger earthquakes.

References

Ambraseys, N., and R. Bilham (2003), Earthquakes and associated deformation in Northern Baluchistan 1892–2001, *Bull. Seismol. Soc. Am.*, *93*(4), 1573–1605.

Avouac, J.-P., F. Ayoub, S. Wei, J.-P. Ampuero, L. Meng, S. Leprince, R. Jolivet, Z. Duputel, and D. Helmberger (2014), The 2013, Mw 7.7 Balochistan earthquake, energetic strike-slip reactivation of a thrust fault, *Earth Planet. Sci. Lett.*, *391*, 128–134, doi:10.1016/j.epsl.2014.01.036.

Barnhart, W. D., G. P. Hayes, R. W. Briggs, R. D. Gold, and R. Bilham (2014), Ball-and-socket tectonic rotation during the 2013 Mw 7.7 Balochistan earthquake, *Earth Planet. Sci. Lett.*, *403*, 210–216, doi:10.1016/j.epsl.2014.07.001.

Bell, J. W., F. Amelung, and C. D. Henry (2012), InSAR analysis of the 2008 Reno-Mogul earthquake swarm: Evidence for westward migration of Walker Lane style dextral faulting, *Geophys. Res. Lett.*, *39*, L18306, doi:10.1029/2012GL052795.

Berardino, P., G. Fornaro, R. Lanari, S. Member, and E. Sansosti (2002), A new algorithm for surface deformation monitoring based on small baseline differential SAR interferograms, *IEEE Trans. Geosci. Remote Sens.*, *40*(11), 2375–2383.

Brooks, B. A., and L. N. Frazer (2005), Importance reweighting reduces dependence on temperature in Gibbs samplers: An application to the coseismic geodetic inverse problem, *Geophys. J. Int.*, *161*(1), 12–20, doi:10.1111/j.1365-246X.2005.02573.x.

Çakir, Z., S. Ergintav, H. Özener, U. Dogan, A. M. Akoglu, M. Meghraoui, and R. Reilinger (2012), Onset of aseismic creep on major strike-slip faults, *Geology*, *40*(12), 1115–1118.

Dee, D. P., et al. (2011), The ERA-Interim reanalysis: Configuration and performance of the data assimilation system, *Q. J. R. Meteorol. Soc.*, *137*(656), 553–597, doi:10.1002/qj.828.

Dolan, J. F., and B. D. Haravitch (2014), How well do surface slip measurements track slip at depth in large strike-slip earthquakes? The importance of fault structural maturity in controlling on-fault slip versus off-fault surface deformation, *Earth Planet. Sci. Lett.*, *388*, 38–47, doi:10.1016/j.epsl.2013.11.043.

Engdahl, E. R., and A. Villaseñor (2002), Global seismicity: 1900–1999, in *International Handbook of Earthquake and Engineering Seismology*, *Int. Geophys.*, vol. 81, chap. 41, pp. 665–690, XV–XVI, Elsevier, New York.

Fattahi, H., and F. Amelung (2013), DEM error correction in InSAR time series, *IEEE Trans. Geosci. Remote Sens.*, *51*(7), 4249–4259, doi:10.1109/tgrs.2012.2227761.

Fattahi, H., and F. Amelung (2014), InSAR uncertainty due to orbital errors, *Geophys. J. Int.*, *199*(1), 549–560, doi:10.1093/gji/ggu276.

Fialko, Y., D. Sandwell, M. Simons, and P. Rosen (2005), Three-dimensional deformation caused by the Bam, Iran, earthquake and the origin of shallow slip deficit, *Nature*, *435*(7040), 295–299, doi:10.1038/nature03425.

Fielding, E. J., P. R. Lundgren, R. Bürgmann, and G. J. Funning (2009), Shallow fault-zone dilatancy recovery after the 2003 Bam earthquake in Iran, *Nature*, *458*(7234), 64–68, doi:10.1038/nature07817.

Freed, A. M. (2007), Afterslip (and only afterslip) following the 2004 Parkfield, California, earthquake, *Geophys. Res. Lett.*, *34*, L06312, doi:10.1029/2006GL029155.

Furuya, M., and S. P. Satyabala (2008), Slow earthquake in Afghanistan detected by InSAR, *Geophys. Res. Lett.*, *35*, L06309, doi:10.1029/2007GL033049.

Hamiel, Y., G. Baer, L. Kalindekafe, K. Dombola, and P. Chindandali (2012), Seismic and aseismic slip evolution and deformation associated with the 2009–2010 northern Malawi earthquake swarm, East African Rift, *Geophys. J. Int.*, *191*, 898–908, doi:10.1111/j.1365-246X.2012.05673.x.

Hearn, E. H., S. McClusky, S. Ergintav, and R. E. Reilinger (2009), Izmit earthquake postseismic deformation and dynamics of the North Anatolian Fault Zone, *J. Geophys. Res.*, *114*, B08405, doi:10.1029/2008JB006026.

Hsu, Y.-J., M. Simons, J.-P. Avouac, J. Galetzka, K. Sieh, M. Chlieh, D. Natawidjaja, L. Prawirodirdjo, and Y. Bock (2006), Frictional afterslip following the 2005 Nias-Simeulue Earthquake, Sumatra, *Science*, *312*(5782), 1921–1926.

Jacobs, A., D. Sandwell, Y. Fialko, and L. Sichoix (2002), The 1999 (Mw 7. 1) Hector Mine, California, earthquake : Near-field postseismic deformation from ERS interferometry, *Bull. Seismol. Soc. Am.*, *92*(4), 1433–1442.

Jolivet, R., P. S. Agram, N. Y. Lin, M. Simons, M. Doin, G. Peltzer, and Z. Li (2014a), Improving InSAR geodesy using global atmospheric models, *J. Geophys. Res. Solid Earth*, *119*, 2324–2341, doi:10.1002/2013JB010588.

Jolivet, R., et al. (2014b), The 2013 Mw 7.7 Balochistan earthquake: Seismic potential of an accretionary wedge, *Bull. Seismol. Soc. Am.*, *104*(2), 1020–1030, doi:10.1785/0120130313.

Kaneko, Y., and Y. Fialko (2011), Shallow slip deficit due to large strike-slip earthquakes in dynamic rupture simulations with elasto-plastic off-fault response, *Geophys. J. Int.*, *186*(3), 1389–1403, doi:10.1111/j.1365-246X.2011.05117.x.

Lawrence, R. D., R. S. Yeats, S. H. Khan, A. Farah, and K. A. DeJong (1981), Thrust and strike slip fault interaction along the Chaman transform zone, Pakistan, *Geol. Soc. London Spec. Publ.*, *9*, 363–370, doi:10.1144/GSL.SP.1981.009.01.33.

Lindsey, E. O., Y. Fialko, Y. Bock, D. T. Sandwell, and R. Bilham (2014), Localized and distributed creep along the southern San Andreas Fault, *J. Geophys. Res. Solid Earth*, *119*, 7909–7922, doi:10.1002/2014JB011275.

Marinkovic, P., and Y. Larsen (2013), Consequences of long-term ASAR local oscillator frequency decay-An empirical study of 10 years of data, Living Planet Symp., Edinburgh, U. K.

Marone, C., C. H. Scholtz, and R. Bilham (1991), On the mechanics of earthquake afterslip, *J. Geophys. Res.*, *96*(B5), 8441–8452, doi:10.1029/91JB00275.

Miyazaki, S., P. Segall, J. Fukuda, and T. Kato (2004), Space time distribution of afterslip following the 2003 Tokachi-Oki earthquake: Implications for variations in fault zone frictional properties, *Geophys. Res. Lett.*, *31*, L06623, doi:10.1029/2003GL019410.

Noda, H., and N. Lapusta (2013), Stable creeping fault segments can become destructive as a result of dynamic weakening, *Nature*, *493*(7433), 518–521, doi:10.1038/nature11703.

Owen, S. E., and R. Bürgmann (2006), An increment of volcano collapse: Kinematics of the 1975 Kalapana, Hawaii, earthquake, *J. Volcanol. Geotherm. Res.*, *150*(1–3), 163–185, doi:10.1016/j.jvolgeores.2005.07.012.

Peltzer, G., P. Rosen, F. Rogez, and K. Hudnut (1998), Poroelastic rebound along the Landers 1992 earthquake surface rupture, *J. Geophys. Res.*, *103*(B12), 30,131–30,145, doi:10.1029/98JB02302.

Perfettini, H., and J.-P. Avouac (2007), Modeling afterslip and aftershocks following the 1992 Landers earthquake, *J. Geophys. Res.*, *112*, B07409, doi:10.1029/2006JB004399.

Podgorski, J., E. H. Hearn, S. McClusky, R. Reilinger, T. Taymaz, O. Tan, M. Prilepin, T. Guseva, and M. Nadariya (2007), Postseismic deformation following the 1991 Racha, Georgia, earthquake, *Geophys. Res. Lett.*, *34*, L04310, doi:10.1029/2006GL028477.

Rosen, P. A., S. Hensley, G. Peltzer, and M. Simons (2004), Updated repeat orbit interferometry package released, *Eos Trans. AGU*, *85*(5), 47, doi:10.1029/2004EO050004.

Scholz, C. H. (1998), Earthquakes and friction laws, *Nature*, *391*, 37–42.

Shen, Z.-K., D. D. Jackson, Y. Feng, M. Cline, M. Kim, P. Fang, and Y. Bock (1994), Postseismic deformation following the Landers earthquake, California, 28 June 1992, *Bull. Seismol. Soc. Am.*, *84*(3), 780–791.

Sun, T., et al. (2014), Prevalence of viscoelastic relaxation after the 2011 Tohoku-Oki earthquake, *Nature*, *514*(7520), 84–87, doi:10.1038/nature13778.

Szeliga, W., R. Bilham, D. M. Kakar, and S. H. Lodi (2012), Interseismic strain accumulation along the western boundary of the Indian subcontinent, *J. Geophys. Res.*, *117*, B08404, doi:10.1029/2011JB008822.

Szeliga, W. M. (2010), Historical and modern seismotectonics of the Indian plate with an emphasis on its western boundary with the Eurasian plate.

Wang, L., R. Wang, F. Roth, B. Enescu, S. Hainzl, and S. Ergintav (2009), Afterslip and viscoelastic relaxation following the 1999 M 7.4 İzmit earthquake from GPS measurements, *Geophys. J. Int.*, *178*(3), 1220–1237, doi:10.1111/j.1365-246X.2009.04228.x.

Wei, M., Y. Kaneko, Y. Liu, and J. J. McGuire (2013), Episodic fault creep events in California controlled by shallow frictional heterogeneity, *Nat. Geosci.*, *6*(7), 566–570, doi:10.1038/ngeo1835.

Weston, J., A. M. G. Ferreira, and G. J. Funning (2011), Global compilation of interferometric synthetic aperture radar earthquake source models: 1. Comparisons with seismic catalogs, *J. Geophys. Res.*, *116*, B08408, doi:10.1029/2010JB008131.

Xu, X., X. Tong, D. Sandwell, T. David, C. Milliner, J. F. Dolan, J. Hollingsworth, S. Leprince, and F. Ayoub (2015), Refining the shallow slip deficit, Fringe 2015 Workshop, Frascati, Italy.